Preparation of Coordination Compounds of Cp^*_2Yb with Heterocyclic Nitrogen Bases: Examples of Antiferromagnetic Exchange Coupling across Bridging Ligands

David J. Berg, James M. Boncella, and Richard A. Andersen*

Chemistry Department and Chemical Sciences Division of Lawrence Berkeley National Laboratory, University of California, Berkeley, California 94720

Received June 19, 2002

Several adducts are isolated between heterocyclic nitrogen bases and Cp^*_2Yb. The adducts fall into several general classes. The membership within the class is related to the reduction potential of the given heterocyclic base relative to that of Cp^*_2Yb. Analytically pure 1:1 adducts of the type $Cp^*_2Yb(L)$ are formed with pyrazine, quinoxaline, 1,5- and 1,8-naphthyridine, and 4,4′-bipyridine as toluene-insoluble solids. The 1:1 adducts with phthalazine and azobenzene and the 1:2 adduct with pyridazine are soluble in toluene, from which they may be isolated by crystallization. All of the adducts in this class are paramagnetic, and their effective magnetic moments are consistent with the formulation $Cp^*_2Yb^{III}(L^{\bullet-})$ ($L^{\bullet-}$ = radical anion), in which spins on the individual units are uncoupled to 5 K. Adducts between Cp^*_2Yb and phenazine, 2,2′-azopyridine, 2,2′-bipyrimidine, 2,2′-azobenzene, and 2,3-bis(2-pyridino)quinoxaline are of 2:1 stoichiometry: $(Cp^*_2Yb)_2(\mu\text{-L})$. The crystal structure of $(Cp^*_2Yb)_2(\mu$-bipyrimidine) shows that the two metallocenes are bridged by a planar bipyrimidine ligand, and the other 2:1 adducts are assumed to have a similar structure. The effective magnetic moment of these 2:1 adducts shows that each $Cp^*_2Yb^{III}$ fragment behaves as an isolated paramagnet and the bridging ligand is a diamagnetic dianion at high temperature. At low temperature the last three adducts undergo antiferromagnetic coupling with a Néel temperature of about 20 K. A spin polarization model is advanced to account for the electronic exchange coupling.

Introduction

The adducts of decamethylytterbocene with pyridine and 2,2′-bipyridine, $Cp^*_2Yb(py)_2$ and $Cp^*_2Yb(bipy)$, respectively, have the same general molecular structures but very different electronic structures. The 1:2 pyridine adduct is green and diamagnetic, while the 1:1 2,2′-bipyridine adduct is brown and paramagnetic.[1,2] The paramagnetism is the result of an electron transfer from the ytterbocene fragment to the LUMO of 2,2′-bipyridine, giving a biradical of the form $Cp^*_2Yb^{III}(bipy^{\bullet-})$, in which the electron spins are correlated in the ground state. The 1:1 1,10-phenanthroline adduct behaves similarly. This paper reports the preparation of a series of adducts of Cp^*_2Yb with heterocyclic nitrogen bases (Chart 1) and the use of variable-temperature magnetic susceptibility measurements to establish the electronic structure of the adducts. A phenomenological understanding of the origin of exchange coupling in those adducts in which two $Cp^*_2Yb^{III}$ fragments undergo antiferromagnetic exchange coupling is also presented.

Results and Discussion

Synthesis and General Physical Properties. The adducts were prepared by adding the nitrogen bases (see Chart 1) to $Cp^*_2Yb(OEt_2)$ in diethyl ether or hydrocarbon solvent. Some physical properties of these adducts are listed in Table 1. In most cases, the adducts were crystallized from the reaction solvent by cooling (see the Experimental Section for details). Several adducts (**1**, **4**, and **5**) are insoluble in hot toluene, although after several washings the powders obtained were analytically pure. The insoluble adduct with 4,4′-bipyridine (**7**) behaves in a curious manner: addition of the base to a toluene solution of $Cp^*_2Yb(OEt_2)$ results in formation of a stiff purple gel. However, removal of the toluene solvent under reduced pressure yields **7** as a free-flowing purple powder that is analytically pure. The adducts do not sublime and generally have very high melting points, although in a few cases it was possible to observe molecular ions in their mass spectrum.

The ^1H NMR spectra of the adducts are a qualitative guide to their net paramagnetism that give an indication of the oxidation state of the ytterbocene fragment (Table 2). The chemical shifts of the Cp* resonances in the diamagnetic adducts appear about δ 2 ppm, and the nitrogen ligand resonances appear near their uncoordinated values. The line width of both sets of resonances are normal (<2 Hz); details can be found in the

* To whom correspondence should be addressed. E-mail: raandersen@lbl.gov.

(1) Tilley, T. D.; Andersen, R. A.; Spencer, B.; Zalkin, A. *Inorg. Chem.* **1982**, *21*, 2647.
(2) Schultz, M.; Boncella, J. M.; Berg, D. J.; Tilley, T. D.; Andersen, R. A. *Organometallics* **2002**, *21*, 460.

10.1021/om020477e CCC: $22.00
Publication on Web 10/03/2002

Chart 1. Nitrogenous Bases Used in This Study

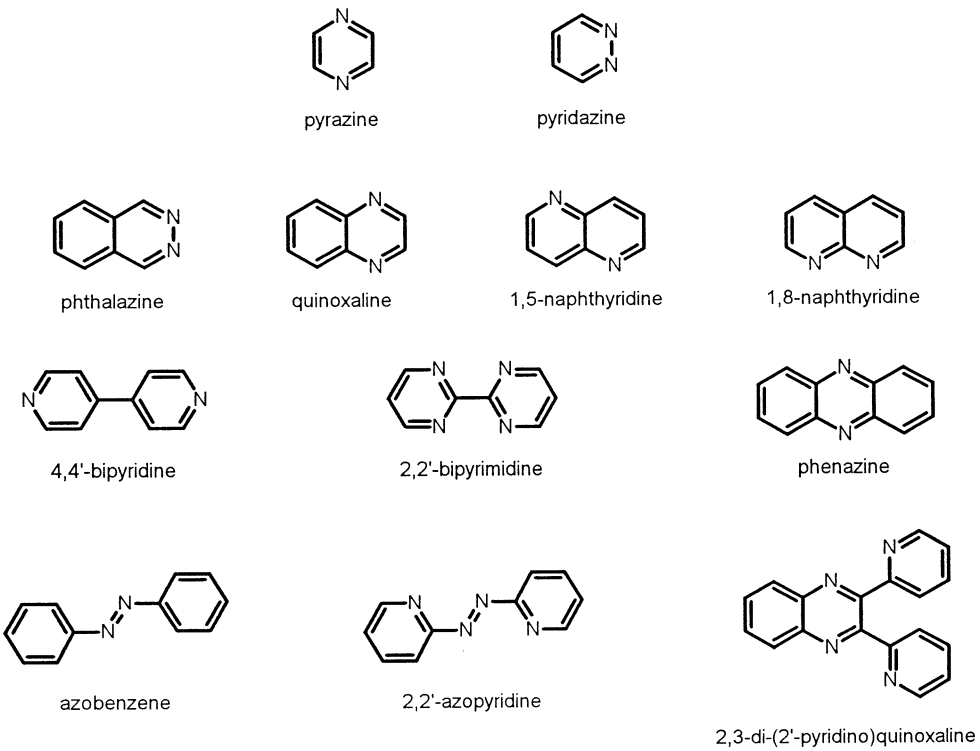

Table 1. General Properties of $[Yb(C_5Me_5)_2]_x[L]_y$ Complexes

						molar magnetic susceptibility μ (μ_B) (Θ (K))[b]	
compd	*x*	*y*	L	color	IR (cm^{-1})[a]	$T = 5-40$ K	$T = 90-300$ K
1	1	1	pyrazine	brown	290	*c*	*c*
2	1	2	pyridazine	red	309	3.37 (−6)	4.49 (−57)
3	1	1	phthalazine	red	311	3.76 (−2)	4.79 (−34)
4	1	1	quinoxaline	brown	294	*c*	*c*
5	1	1	1,5-naphthyridine	brown	303	*c*	*c*
6	1	1	1,8-naphthyridine	red	310	3.72 (−2)	4.29 (−26)
7	1	1	4,4′-bipyridine	purple	290	2.91 (−7)	4.64 (−89)
8	2	1	2,2′-bipyrimidine	dark brown	303	*d*	5.97 (−15)
9	2	1	phenazine	red-brown	315	5.55 (−3)	6.12 (−25)
10	1	1	azobenzene	blue-green	314	3.80 (−5)	4.90 (−25)
11	2	1	azobenzene	dark purple	299	*d*	5.95 (−25)
12	2	1	2,2′-azopyridine	brown-black	301	5.40 (−4)	6.18 (−32)
13	2	1	2,3-bis(2′-pyridino)- quinoxaline	black	305	*d*	5.75 (−16)

[a] Strong-intensity ring tilt vibration; recorded as Nujol mulls on CsI plates. [b] Recorded between 5 and 40 kG field strength in the solid state and expressed as moment per Yb(III). [c] Not measured. [d] Antiferromagnetic coupling was observed in this temperature regime.

Table 2. ^{1}H NMR Data for Paramagnetic $[Yb(C_5Me_5)_2]_x[L]_y$ Complexes

				^{1}H NMR (δ)[a]	
compd	*x*	*y*	L	C_5Me_5	ligand
3	1	1	phthalazine	31.2 (30H, 51)	-3.7 (1H, 15), −9.1 (1H, 17), −9.5 (1H, 14), −15.0 (1H, 27)
6	1	1	1,8-naphthyridine	7.9 (30H, 200)	-1.1 (1H, 16), −7.9 (1H, 15), −8.6 (1H, 17), −9.3 (1H, 19), −23.8 (1H, 26)[b]
8	2	1	2,2′-bipyrimidine	-4.1 (60H, 61)	68.5 (2H, 28), 4.2 (4H, 103)
9	2	1	phenazine	-1.9 (60H, 380)	6.4 (4H, 16), 5.6 (4H, 16)
10	1	1	azobenzene	14.1 (30H, 25)	79.1 (4H, 24), −145.9 (4H, 230), −186.6 (2H, 97)
11	2	1	azobenzene	-5.8 (60H, 300)	18.1 (4H, 12), 11.4 (4H, 20), −15.7 (2H, 16)
12	2	1	2,2′-azopyridine	-2.1 (30H, 163), −12.6 (30H, 86)	74.2 (2H, 40), 61.4 (2H, 35), 18.3 (2H, 21)[b]
13	2	1	2,3-bis(2′-pyridino)quinoxaline	-6.0 (30H, 100), -6.8 (30H, 100)	108.9 (2H, 64), 71.8 (2H, 54), 29.6 (2H, 29), −22.0 (2H, 29)[b]

[a] Recorded in d_6-benzene or d_8-toluene at 32 °C. The relative intensity and line width at half peak height (Hz) are given in parentheses. [b] The remaining ligand resonances were not observed.

Experimental Section. In the paramagnetic species, the Cp* resonances range from δ 31 to −13 ppm and the peak width (full width at half-height) ranges from 25 to 380 Hz. The chemical shifts of the ligand resonances occur over a wide range, as do the peak widths; in some cases not all of the ligand resonances are observed.

Table 1 also lists a stretching frequency in the low-energy range of the infrared spectrum that gives

another indication of the oxidation state of the ytterbium center in the adducts. The empirical observation is that adducts containing a $Cp^*_2Yb^{II}$ fragment have a strong band in the 265−275 cm^{-1} range, while those containing a $Cp^*_2Yb^{III}$ fragment exhibit a band between 290 and 315 cm^{-1}.[3] This absorption has been assigned to the Cp−M−Cp ring-tilting motion in p- and d-block metallocenes.[4] It is reasonable that this vibration occurs at higher frequencies for Yb(III) metal centers, because the stronger metal−ring bonding in the higher oxidation state makes the ring-tilting vibration more difficult and therefore higher in energy.

General Systematics. Adducts of Six-Membered Cyclic Rings with Two Nitrogen Atoms. The paramagnetic 1:2 adduct with pyridazine, $Cp^*_2Yb(pyridazine)_2$ (**2**), has the same stoichiometry, and presumably a similar structure, as the diamagnetic adduct with pyridine, $Cp^*_2Yb(py)_2$ (**1**). It is noteworthy that Cp^*_2Sm yields a complex with the stoichiometry $[Cp^*_2Sm(THF)(pyridazine)]_2$, which results from radical coupling of the pyridazine at the 4,4′-carbon positions.[5] It is not clear why the net reactions of these two lanthanide metallocenes with pyridazine are so different, but it seems reasonable to speculate that the odd electron on the base residue in a 1:1 adduct (Sm case) has a higher spin density in the para position than is found in the 1:2 adduct (Yb case) and this results in rapid C−C bond formation in the samarium complex.

The adduct with pyrazine, **1**, has a 1:1 stoichiometry and is insoluble in hot toluene, presumably indicating a polymeric structure. Like the pyrazine complex **1**, phthalazine yields a 1:1 paramagnetic adduct, **3**; however, in this case the complex is soluble in toluene. The ^1H NMR spectrum at 30 °C shows two widely separated Cp* resonances, but only four of the six base protons were located (Table 2). The variable-temperature ^1H NMR spectrum shows the normal temperature dependence for the chemical shifts of the Cp* resonances, indicating that there are no dynamic processes occurring that average the Cp* resonances to 120 °C. The structure of this adduct cannot be the expected one with idealized C_{2v} symmetry, unless the heterocycle is nonplanar or lies in the plane perpendicular to the metallocene fragment. Both of these possibilities are unlikely, since dynamic behavior in solution should be rapid and would lead to an average C_{2v} structure. Two structural possibilities may be advanced to account for the NMR data. The first postulates that two paramagnetic fragments dimerize, as illustrated in eq 1. The structure of the dimer will have idealized C_{2h} symmetry, since the two heterocyclic rings are no longer planar and no symmetry operation interconverts the Cp* rings on a given ytterbium center. This structural possibility is thus related to that observed in the solid state for $Cp^*_4Sm_2(pyridazine)_2(THF)_2$ mentioned above.[5] The other possibility is that two distinct Cp^*_2Yb fragments are present in an ion-pair structure similar to that illustrated in eq 2. The adduct is reasonably soluble in toluene, which seems to favor the dimer shown in eq 1 over the charged species shown in eq 2; however, in the absence of a crystal structure, these structural possibilities remain conjecture. At this point, all that can be said with confidence is that the complex contains two $Cp^*_2Yb^{III}$ fragments and that the magnetic susceptibility is normal (see below).

$$2\ Cp^*_2Yb(III)(phthalazine) \rightleftharpoons Cp^*_4Yb(III)_2(phthalazine)_2 \qquad (1)$$

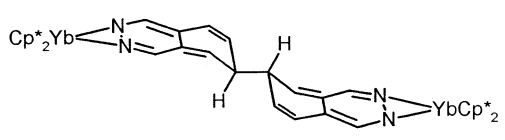

$$2\ Cp^*_2Yb(III)(phthalazine) \rightleftharpoons [Cp^*_2Yb(III)(phthalazine)]^+\ [Cp^*_2Yb(III)(phthalazine^{2-})]^- \qquad (2)$$

The 1:1 quinoxaline adduct **4** is insoluble in toluene, just like the 1:1 adduct with pyrazine **1**. The 1,5-naphthyridine adduct **5** is also insoluble in toluene, and both are likely to have a polymeric constitution. In contrast, the 1,8-naphthyridine adduct **6** is soluble in toluene and crystallizes from that solvent. This 1:1 adduct is paramagnetic in solution and in the solid state (Table 1).

The phenazine adduct **9** is quite different from that formed by quinoxaline **4**, as it dissolves in toluene and has a 2:1 stoichiometry $(Cp^*_2Yb)_2(phenazine)$, the first complex with this stoichiometry encountered in this work; additional examples of this stoichiometry are described below. The Cp* rings are equivalent in solution and the magnetic moment is consistent with two Yb(III) centers (Table 1), suggesting that the phenazine ligand is present as a dianion.

Adducts of Six-Membered Cyclic Rings with Four Nitrogen Atoms. 2,2′-Bipyrimidine forms another example of an adduct with 2:1 stoichiometry, **8**. This adduct crystallizes as dark purple crystals from toluene, and the mass spectrum supports a 2:1 metal-to-ligand ratio. The ^1H NMR spectrum shows a single paramagnetically shifted Cp* resonance and two bipyrimidine ring resonances in a 2:1 ratio, consistent with a structure of C_{2v} symmetry (Table 2). This deduction is confirmed by a single-crystal X-ray structural determination. The ORTEP[6] diagram is shown in Figure 1, in which a disordered toluene of solvation has been omitted. Full crystallographic details are given in Table 3. The molecule crystallizes in the triclinic space group $P\bar{1}$ with two molecules in the unit cell. Three of the four Cp* rings are disordered, and the carbon atoms are constrained and refined isotropically. The Yb−C distances range from 2.57 to 2.69 Å; the distances do not carry much statistical significance, due to the disorder. The bridging bipyrimidine carbon and nitrogen atoms do not seem to be affected by the disorder in the Cp* rings, since they can be refined anisotropically, although the hydrogen atoms associated with the carbon atoms were neither located nor refined.

(3) Burns, C. J. Ph.D. Thesis, University of California, Berkeley, CA, 1987.

(4) Aleksanyan, V. T. In *Vibrational Spectra and Structure*; Durig, J. R., Ed.; Elsevier: Amsterdam, 1982; pp 115−144.

(5) Evans, W. J.; Drummond, D. K. *J. Am. Chem. Soc.* **1989**, *111*, 3329.

(6) Johnson, C. K. ORTEP; Report ORNL-3794; Oak Ridge National Laboratory, Oak Ridge, TN, 1965.

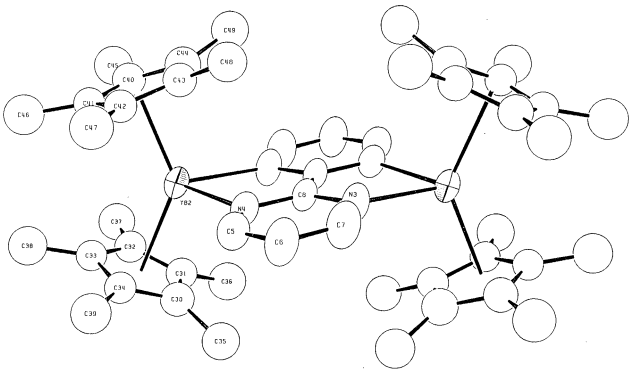

Figure 1. ORTEP drawing of $[(Me_5C_5)_2Yb]_2$(2,2′-bipyrimidine)·toluene (**8**). The disordered toluene of crystallization is not shown. Three of the four Me_5C_5 rings are disordered; all of the carbon atoms are shown as isotropic spheres of 50% probability. The carbon and nitrogen atoms of the bipyrimidine ring were refined anisotropically, but the hydrogen atoms were not located.

Table 3. Summary of Crystallographic Data[a]

	2,2′-bipyrimidine	**8**·(toluene)
formula	$C_8H_6N_4$	$C_{55}H_{74}N_4Yb_2$
fw	158.1	1137.3
cryst size (mm)	0.21 × 0.23 × 0.40	0.34 × 0.24 × 0.20
cryst syst	monoclinic	triclinic
space group	$P2_1/n$ (No. 14)	$P\bar{1}$ (No. 2)
a (Å)	3.8567(4)	10.5037(9)
b (Å)	10.796(2)	11.233(1)
c (Å)	8.844(1)	22.203(2)
α (deg)	90	93.248(9)
β (deg)	101.028(10)	90.529(7)
γ (deg)	90	102.519(8)
V (Å^3)	361.4	2553
Z	2	2
ρ(calcd) (g cm^{-3})	1.453	1.48
μ (cm^{-1})	0.9	36.67
temp (K)	163	295
$2\theta_{max}$ (deg)	55	45
no. of rflns collected	1997	6654
no. of unique rflns	932	6654
no. of rflns with $I > 3.0\sigma(I)$	746	5707
R	0.031	0.030
R_w	0.047	0.049
GOF on F^2	2.141	2.51

[a] Data were collected on an Enraf-Nonius CAD4 diffractometer equipped with graphite-monochromated Mo Kα radiation (λ = 0.710 73 Å) at the temperatures indicated.

Table 4. Comparison of Ring C−C and C−N Bond Distances (Å) in 8 and Free 2,2′-Bipyrimidine

bond	**8**	2,2′-bipm	Δ(complex − free)
N1−C1	1.416(10)	1.336(1)	0.080
N2−C1	1.428(3)	1.335(1)	0.093
N2−C4	1.306(11)	1.341(1)	-0.035
N1−C2	1.320(5)	1.336(1)	-0.016
C2−C3	1.407(12)	1.373(1)	0.034
C3−C4	1.400(13)	1.374(1)	0.022
C1−C1′	1.359(1)	1.501(1)	−0.142

To determine how the bond lengths within the bridging ligand change in the adduct relative to the free base, a low-temperature (−105 °C) data set (2θ to 55°) was collected for the free base. An ORTEP[6] diagram is shown in Figure 2, and crystal data are collected in Table 3. All of the non-hydrogen atoms were refined anisotropically, and the hydrogen atoms were located and refined isotropically. A comparison of the C−C and C−N distances in the two structures is shown in Table 4. Examination of these data shows that the distances tend to elongate and contract in a systematic manner and these distortions range from being just on the edge of statistical significance to being highly significant for the C(1)−C(1′) distance. These bond length changes can be rationalized by postulating that the bipyrimidine ligand is a dianion and that the two electrons are paired in the LUMO of bipyrimidine. This orbital has b_{1u} symmetry in the D_{2h} point group and is represented schematically by **A**, with shaded and unshaded circles representing the phase of the pπ orbitals at each carbon. An alternative valence bond representation is shown by **B**.

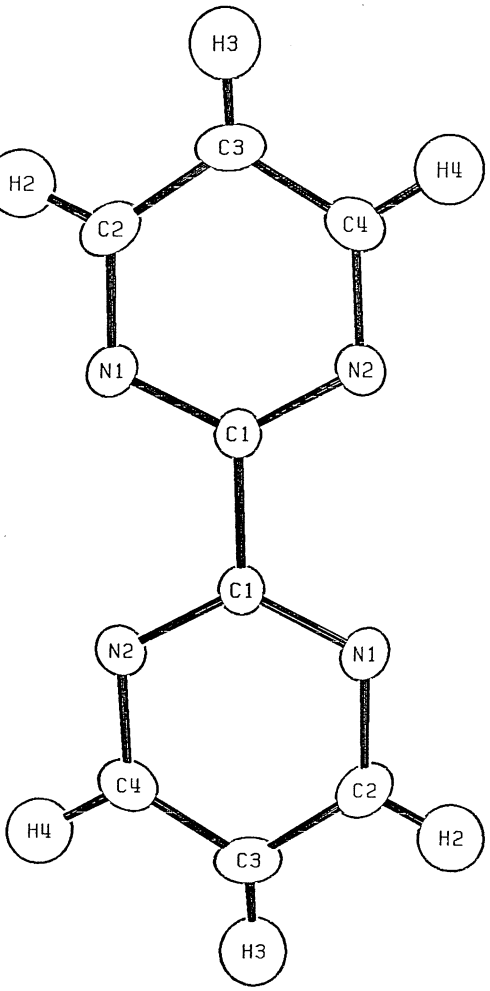

Figure 2. ORTEP drawing (50% probability ellipsoids) of 2,2′-bipyrimidine. The carbon and nitrogen atoms were refined anisotropically, and the hydrogen atoms were refined isotropically.

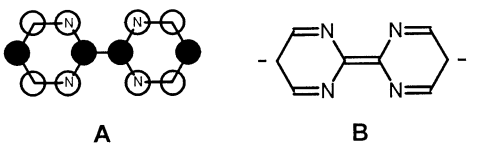

2,3-Bis(2′-pyridino)quinoxaline also gives a 2:1 adduct with Cp^*_2Yb, **13**. This adduct is soluble in toluene, and

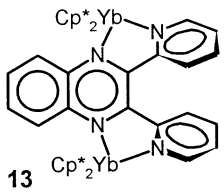

13

the ^{1}H NMR spectrum shows two equal-intensity resonances for the Cp* groups (Table 2). Although the solid-state structure of this compound is unknown, the two inequivalent Cp* resonances are consistent with averaged C_2 symmetry, suggesting a structure such as that shown. Heating a ^{1}H NMR sample of **13** results in coalescence of the Cp* resonances at 120 °C, corresponding to a $\Delta G^{\ddagger}$ value of 20 kcal mol^{-1}. The simplest process to explain Cp* site exchange at high temperature (120 °C) is dissociation of the 2-pyridyl groups to generate a complex with averaged C_{2v} symmetry.

Adducts with Azobenzene and Derivatives. Azobenzene forms two isolable adducts with Cp*$_2$Yb. Reaction of Cp*$_2$Yb(OEt$_2$) with 1 equiv of azobenzene affords a blue-green solution from which a 1:1 adduct is isolated upon cooling, **10**. When 2 equiv of Cp*$_2$Yb(OEt$_2$) is added to a solution of azobenzene, a dark purple solution is formed from which the 2:1 adduct **11** is isolated on cooling. The NMR spectrum of **10** shows that it is paramagnetic, and the mass spectrum indicates that it is monomeric; thus, this complex is most reasonably formulated as an adduct between Cp*$_2$Yb^{III} and a Ph_2N_2 radical anion. The infrared spectrum of **10** is consistent with the presence of a *cis*-azobenzene unit, since the complex shows four strong absorptions between 650 and 800 cm^{-1} (680, 701, 750, and 783 cm^{-1}). Similarly free *cis*-azobenzene also has four absorptions in this region (689, 701, 757, and 779 cm^{-1}) while the trans isomer has only two (687 and 771 cm^{-1}).[7,8]

The 2:1 adduct is also paramagnetic, and a structure based upon two Cp*$_2$Yb^{III} fragments bridged by a *trans*-Ph_2N_2 dianion is proposed. The crystal structure of a 2:1 adduct between Cp*$_2$Sm and azobenzene has just this structure, and the infrared spectrum of **11** is identical with that reported for the samarium analogue.[8] The adduct **11** has a formal relationship to **9** and **13**, as they all have two Cp*$_2$Yb^{III} units that bridge dianionic nitrogen bases. However, the magnetic behavior of these three complexes is different: in **9**, the two Yb(III) fragments behave as independent paramagnets, whereas those two fragments in **11** and **13** do not. The magnetic behavior of these complexes is examined in the following section.

Variable-Temperature Magnetic Susceptibility. The free ion spectroscopic term symbol for a 4f^{13} ion is $^2F_{7/2}$, and the expected magnetic moment is 4.5 μ_B. When the ion is surrounded by ligands and the complex is placed in a magnetic field, the degeneracy of the crystal field states is removed. In low symmetry, four Kramers doublets will result and all states will be populated at 300 K, resulting in an effective magnetic moment that approaches the free ion value.[9−12] In isolated metallocenes and other compounds of Yb(III), the temperature dependence of the magnetic susceptibility follows the Curie−Weiss law ($C = \chi(T - \Theta)$) from about 100 to 300 K with Θ values in the range −20 to −90 K. The effective magnetic moment is very close to the predicted value of 4.5 μ_B, since the ligand field splitting of the ground-state term is smaller than kT over this temperature range.[13] As the temperature is lowered, the population of the Kramers doublet states change so that at low temperature only the lowest two states are appreciably occupied and contribute to the magnetic moment. In the low-temperature range (5−30 K), the magnetic susceptibility follows the Curie law ($C = \chi T$) with an effective magnetic moment of about 3.8 μ_B.[14,15]

A plot of the inverse of the molar susceptibility (χ^{-1}) as a function of temperature for magnetically dilute Yb(III) compounds therefore has two linear regions. The slope ($1/C$) of each region is directly related to the effective magnetic moment, $\mu = 2.828C^{1/2}$. For a Cp*$_2$Yb^{III}X compound where X is a closed-shell univalent anion (free or bound), a plot of χ^{-1} vs T is linear from 5 to 30 K and from 90 to 300 K and the effective magnetic moments are 3.8 and 4.5 μ_B, respectively.[14] In the paramagnetic 1:1 Cp*$_2$Yb complexes described in this paper, complications arise, since the heterocyclic amine base is a radical anion and the spin carriers can either communicate with one another or not. In the case of no communication, the effective magnetic moment is the root mean square (RMS) value of the individual magnetic moments. This is because the total susceptibility (χ_T) is the sum of the individual susceptibilities, $\chi_T = \chi_1 + \chi_2 + \chi_3 + ...$; thus, $\chi_T T = \chi_1 T + \chi_2 T + \chi_3 T + ...$ and, since $\mu^2 = (2.828)^2(\chi T)$, then $\mu_T^2 = \mu_1^2 + \mu_2^2 + \mu_3^2 + ...$ and $\mu_T = (\mu_1^2 + \mu_2^2 + \mu_3^2 + ...)^{1/2}$. Since the magnetic moment of a free radical with $S = {}^1/_2$ is 1.73 μ_B, the expected magnetic moments for a Yb(III) complex that also contains a noninteracting radical anion are about 4.2 and 4.8 μ_B in the 5−30 and 90−300 K temperature ranges, respectively. In cases where the spin carriers interact antiferromagnetically, the observed magnetic moments are much lower than predicted on the basis of the preceding discussion and the shapes of the χ vs T plots are very different.[2,16,17] In the 1:1 adducts described here, the χ^{-1} vs T plots are normal for **2**, **3**, **6**, and **7** (Table 1) down to 5 K, indicating that no antiferromagnetic interaction is occurring between the spin carriers in this temperature regime.

In the case of two isolated Cp*$_2$Yb^{III} units bridged by a diamagnetic linking group, the expected effective magnetic moment is the RMS value of the individual magnetic moments, which corresponds to values of 5.4 and 6.4 μ_B in the low- and high-temperature regions, respectively. This behavior is observed for **9** and **12**, as illustrated by the χ^{-1} vs T plots in Figures 3 and 4. These curves are similar to those in which the bridging groups are the dinegative elements oxygen, sulfur, selenium, and tellurium,[13] in which no magnetic exchange interaction was observed down to 5 K. In

(7) Gruger, A.; LeCalvé, N.; Fillaux, J. *J. Chim. Phys.* **1972**, *69*, 743.
(8) Evans, W. J.; Drummond, D. K.; Chamberlain, L. R.; Doedens, R. J.; Bott, S. G.; Zhang, H.; Atwood, J. L. *J. Am. Chem. Soc.* **1988**, *110*, 4983.
(9) Van Vleck, J. J. *The Theory of Electronic and Magnetic Susceptibilities*; Clarendon Press: Oxford, U.K., 1932.
(10) Boudreaux, E. M.; Mulay, L. N. *Theory and Applications of Molecular Paramagnetism*; Wiley: New York, 1976.
(11) Edelstein, N. M. In *Organometallics of the f-Elements*; Marks, T. J., Fischer, R. D., Eds.; D. Reidel: Dordrecht, Holland, 1979; p 37.
(12) Edelstein, N. M. In *Fundamental and Technological Aspects of Organo-f-Element Chemistry*; Marks, T. J., Fragala, I. L., Eds.; Reidel: Dordrecht, Holland, 1985; p 229.
(13) Figgis, B. N. *Introduction to Ligand Fields*; Wiley: New York, 1966.
(14) Berg, D. J.; Burns, C. J.; Andersen, R. A.; Zalkin, A. *Organometallics* **1989**, *8*, 1865.
(15) Bochkarev, M. N.; Trifonov, A. A.; Cloke, F. G. N.; Dalby, C. I.; Matsunaga, P. T.; Andersen, R. A.; Schumann, H.; Loebel, J.; Hemling, H. *J. Organomet. Chem.* **1995**, *486*, 177.
(16) Kahn, M. L.; Sutter, I.-P.; Golhen, S.; Gnionnean, P.; Onahab, L.; Kahn, O.; Chasseau, D. *J. Am. Chem. Soc.* **2000**, *122*, 3413.
(17) Costes, J.-P.; Dahan, F.; Dupuis, A.; Laurent, J.-P. *Chem Eur. J.* **1998**, *4*, 1616.

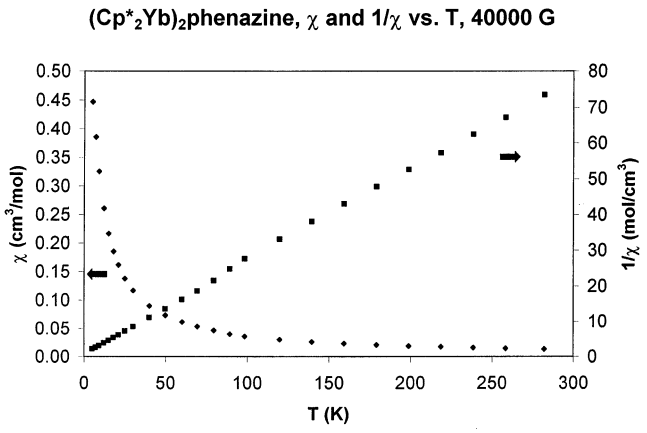

Figure 3. χ_M and $1/\chi_M$ versus temperature plots for **9** at 40 kG.

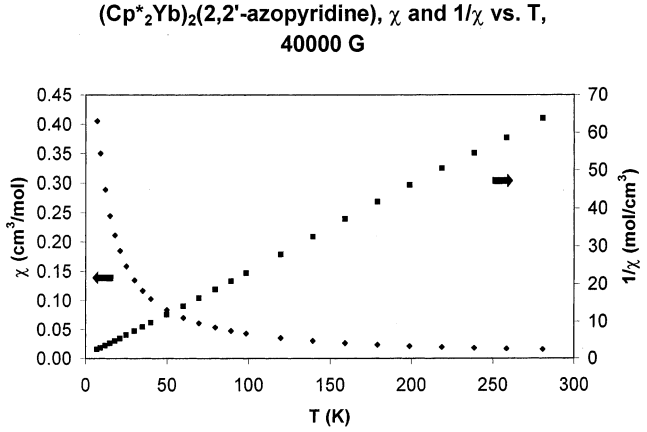

Figure 4. χ_M and $1/\chi_M$ versus temperature plots for **12** at 40 kG.

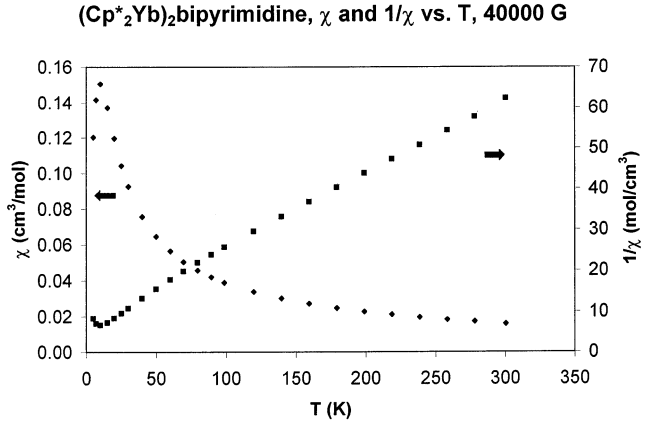

Figure 5. χ_M and $1/\chi_M$ versus temperature plots for **8** at 40 kG.

contrast, **8**, **11**, and **13** behave differently at low temperature (Figures 5−7). At high temperature, the plots of χ^{-1} vs T are as expected for two uncorrelated spin carriers and yield effective magnetic moments of about 6 μ_B (Table 1). However, at low temperature the value of χ_M increases normally with decreasing temperature until a maximum is reached and then declines rapidly with decreasing temperature. This behavior is the signature of an antiferromagnetic spin exchange interaction, and the temperature at which maximum susceptibility occurs (Néel temperature) varies from a low of 12 K in **8** to 15 K in **9** and a high of 18 K in **13**.

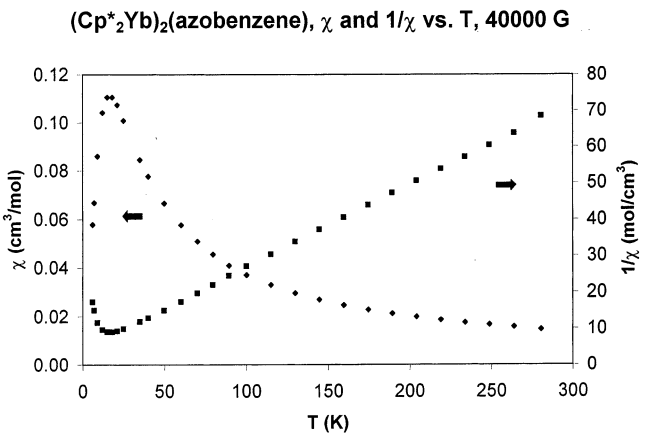

Figure 6. χ_M and $1/\chi_M$ versus temperature plots for **11** at 40 kG.

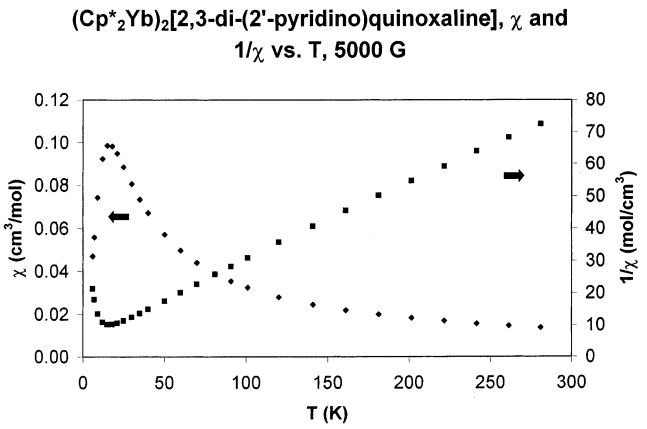

Figure 7. χ_M and $1/\chi_M$ versus temperature plots for **13** at 40 kG.

Antiferromagnetic coupling between two $(MeC_5H_4)_3U^V$ fragments across a diamagnetic dianionic bridging ligand has been observed where the Néel temperature is approximately 20 K, and a coupling constant (J) of about 20 cm^{-1} was extracted using an Ising model.[18] Thus, in all cases so far reported that involve antiferromagnetic coupling of a $4f^{13}$ or $5f^1$ electron across a diamagnetic bridging ligand, the coupling constants are of comparable magnitude. A reasonable microscopic explanation for the coupling is a polarization model, which is an electrostatic model that introduces spin correlation through polarization, rather than a molecular orbital model that introduces spin correlation through orbitals.[19,20] It is impossible to decide which model is a better one, but the polarization model has the virtue that it is simple to use and understand.

The polarization model is applied to **8** in the following way. In a linear arrangement, Yb(1)−L−Yb(2), where Yb symbolizes $Cp^*_2Yb^{III}$ and L symbolizes the bridging dianionic ligand, the spins on the two Yb(III) fragments can be oriented in two ways: Yb(α)···Yb(α) and Yb(α)···Yb(β). When the spin-paired bridging group, symbolized by L($\alpha\beta$), is placed between the two Yb(III) fragments, four possible arrangements of the four spins will

(18) Rosen, R. K.; Andersen, R. A.; Edelstein, N. M. *J. Am. Chem. Soc.* **1990**, *112*, 4588.
(19) Drago, R. S. *Physical Methods in Chemistry*; Sanders: Philadelphia, 1977; p 329.
(20) Carrington, A.; McLachlain, A. D. *Introduction to Magnetic Resonance*; Harper and Row: New York, 1967; p 81.

Table 5. Reduction Potentials (V) of Several Nitrogenous Bases[a]

base	$-\epsilon_{1/2}^1$	$-\epsilon_{1/2}^2$	ref
pyridine	2.6		24−27
pyridazine	2.2		24−27
quinoline	2.1		25−27
pyrazine	2.1		24−27
phthalazine	2.0		25−27
4,4′-bipyridine	1.9		27, 28
quinoxaline	1.8	2.2	25−27
1,5-naphthyridine	1.8		27
2,2′-bipyrimidine	1.8	2.4	29, 30
azobenzene	1.4	2.0	26, 27, 31
phenazine	1.2	1.8	25−27
2,2′-azopyridine	1.0	1.6	27, 32

[a] Relative to the saturated calomel electrode (SCE) in acetonitrile or dimethylformamide.

result: α(α*β*)*β*, α(*β*α)α, α(α*β*)*β*, and α(*β*α)*β*. The difference in energy between these states is small, and the state with the α(α*β*)*β* orientation is slightly preferred, since there are two favorable exchange interactions between spins on the Yb(III) fragments with the spins on the bridging ligand. The spins are therefore polarized, with the result that the spin on each Yb(III) is antiferromagnetically aligned below the Néel temperature. Increasing the temperature results in population of the other spin alignments, and χ increases with temperature until the populations of each state are equal (Néel temperature). At higher temperatures, χ decreases with increasing temperature, since the spins are uncorrelated.

An interesting question is why antiferromagnetic coupling is observed in **8** but not for **9**. Qualitatively, this is related to the energy and symmetry of the orbital that is occupied by the pair of electrons in the bridging ligand. In the nitrogen heterocyclic bases, these orbitals are C−C and C−N antibonding and the orbital energies are relatively high so the electrons in these orbitals can be polarized. The converse is presumably the reason no antiferromagnetic coupling is observed in $(Cp^*_2Yb)_2(\mu$-E) (E = O, S, Se, Te):[13] viz., the orbital energy of the nonmetal dianion is too far away from that of the $Cp^*_2Yb^{III}$ fragment and polarization effects are small. These ideas, though qualitative, are useful since they provide a guide to additional experiments.

The ability of the heterocyclic base to accept one or two electrons is related to its reduction potential; reduction potentials of bases used in this study are collected in Table 5. The reduction potential of Cp^*_2Yb in MeCN is −1.4 V (vs SCE).[22,23] Thus, on the basis of the reported reduction potential of Cp^*_2Yb, very few of these nitrogen bases should be reduced, although many clearly are. When a ligand binds to an electron-poor metal, its reduction potential is presumably lowered. In the present case, the extent to which the reduction potentials of the heterocyclic bases are lowered by coordination may be estimated in the following way. Pyridine ($\epsilon^\circ = -2.6$ V) yields a diamagnetic 1:2 adduct, but pyridazine ($\epsilon^\circ = -2.2$ V) yields a 1:2 adduct which contains a "normal" $Cp^*_2Yb^{III}$ fragment. Thus, it appears that when the reduction potential of the ligand is about −2.2 V or less, Cp^*_2Yb can reduce it. In those ligands which have at least two nitrogen atoms that are sterically accessible to a Cp^*_2Yb fragment, transfer of two electrons to form a dianion occurs if the reduction potential of the ligand is on the order of −2.4 V or less. This is the thermodynamic condition, and it assumes that the kinetics of electron transfer are rapid. Once the two electrons are in a singlet state, their polarizability determines whether the two $Cp^*_2Yb^{III}$ fragments communicate electronically. In those cases where the second reduction potential is known (Table 5), antiferromagnetic coupling results when this value is more negative than about −2 V, as in azobenzene and 2,2′-bipyrimidine. When the potential is less negative, as in the case of phenazine, no coupling results. These ideas are in accord with the polarization model advanced above.

Conclusions

The paramagnetic adducts between Cp^*_2Yb and heterocyclic nitrogen bases described in this paper may be classified in the following manner, as derived from the temperature dependence of the magnetic susceptibility. **Class 1**: the 1:1 and 1:2 adducts exhibit magnetic susceptibility curves that show the spins to be uncorrelated to 5 K. Examples of this class include **1**−**7** and **10** (Table 1). **Class 2**: the 2:1 adducts in which each $Cp^*_2Yb^{III}$ fragment is linked by a dianionic diamagnetic bridging group with no magnetic exchange occurring between the spin carriers to 5 K. Examples of this class include **9** and **12**. The bridging chalcogenide compounds $(Cp^*_2Yb)(\mu$-E) (E = O, S, Se, Te) also fall into this class.[13] **Class 3**: adducts with 2:1 stoichiometry but containing $Cp^*_2Yb^{III}$ fragments that couple antiferromagnetically at low temperature. Examples of this class include **8**, **11**, and **13**, in which the Néel temperature is between 12 and 18 K.

Experimental Section

General Procedures. All solvents were dried and deoxygenated by distillation from sodium benzophenone ketyl under nitrogen prior to use. 1,8-Naphthyridine,[33] 2,2′-azopyridine,[34] and 2,3-bis(2′-pyridino)quinoxaline[35] were prepared according to literature procedures; the remaining nitrogen bases were purchased commercially. Liquid nitrogen bases were generally purified and dried by vacuum distillation from BaO prior to use. Solid bases were purified by recrystallization or sublimation. $Yb(C_5Me_5)_2(OEt_2)$ was prepared according to a published procedure.[36] All reactions were carried out using standard

(21) Bordon, W. T. *Diradicals*; Wiley: New York, 1982; p 11.
(22) Salem, L. *Electrons in Chemical Reactions*; Wiley: New York, 1982; p 188.
(23) Finke, R. G.; Keenan, S. R.; Schiraldi, D. A.; Watson, P. L. *Organometallics* **1986**, *5*, 598.
(24) O'Reilly, J. E.; Elving, P. J. *J. Am. Chem. Soc.* **1972**, *94*, 7941.
(25) Maruyama, M.; Murakami, K. *J. Electroanal. Chem. Interfacial Electrochem.* **1979**, *102*, 221.
(26) Millefiori, S. *J. Heterocycl. Chem.* **1970**, *7*, 145.
(27) Tabner, B. J.; Yandle, J. R. *J. Chem. Soc. A* **1968**, 381.
(28) Creutz, C. *Comments Inorg. Chem.* **1982**, *1*, 293.
(29) Geske, D. H.; Padmanabhan, G. R. *J. Am. Chem. Soc.* **1965**, *87*, 1651.
(30) Ernst, S.; Kaim, W. *J. Am. Chem. Soc.* **1986**, *108*, 3578.
(31) Lines, R.; Jensen, B. S.; Parker, V. D. *Acta Chim. Scand., Ser. B* **1978**, *32*, 510.
(32) Bellamy, A. J.; MacKirdy, I. S.; Niven, C. A. *J. Chem. Soc., Perkin Trans. 2* **1983**, 183.
(33) (a) Paudler, W. W.; Kress, T. J. *J. Org. Chem.* **1967**, *32*, 832. (b) Utermohlen, W. P. *J. Org. Chem.* **1943**, *8*, 544.
(34) Campbell, N.; Henderson, A. W.; Taylor, D. *J. Chem. Soc.* **1953**, 1281.
(35) Goodwin, H. A.; Lions, F. *J. Am. Chem. Soc.* **1959**, *81*, 6415.
(36) Tilley, T. D.; Boncella, J. M.; Berg, D. J.; Burns, C. J.; Andersen, R. A. *Inorg. Synth.* **1990**, *27*, 146.

Schlenk techniques under an atmosphere of dry nitrogen as previously described.[14]

Yb(C_5Me_5)$_2$(pyrazine)·(toluene) (1). A solution of pyrazine (0.060 g, 0.80 mmol) dissolved in 20 mL of toluene was added to a solution of Yb(C_5Me_5)$_2$(OEt_2) (0.84 g, 1.6 mmol) in 40 mL of toluene by cannula. The solution turned brown immediately and slowly deposited a brown microcrystalline solid. The precipitate was isolated by cannula filtration, washed repeatedly with hexane, and dried under reduced pressure to afford **1** as a highly pyrophoric brown powder. A second crop was obtained by cooling the filtrate from the initial reaction mixture to −10 °C. Yield: 0.55 g (56%). Mp: >330 °C. Anal. Calcd for $C_{24}H_{34}N_2Yb$: C, 60.5; H, 6.88; N, 4.55. Found: C, 59.7; H, 6.82; N, 4.22. IR (cm^{-1}): 3180 (br w), 2725 (m), 1005 (s), 970 (w), 755 (m), 720 (vs), 690 (w), 460 (w), 400 (br s), 290 (vs).

Yb(C_5Me_5)$_2$(pyridazine)$_2$ (2). Neat pyridazine (0.20 mL, 2.2 mmol) was added to a solution of Yb(C_5Me_5)$_2$(OEt_2) (0.51 g, 0.99 mmol) in 100 mL of diethyl ether by syringe. The resulting deep red solution was stirred for 2 h and the solution cooled overnight at −10 °C. Dark red crystals were isolated from the mother liquor by cannula filtration, but these immediately collapsed to a rust-colored powder on exposure to vacuum. Powdered samples of **2** were only sparingly soluble in toluene or diethyl ether. Yield: 0.45 g (75%). Mp: 176−177 °C. Anal. Calcd for $C_{28}H_{38}N_4Yb$: C, 55.7; H, 6.34; N, 8.93. Found: C, 55.8; H, 6.72; N, 8.84. IR (cm^{-1}): 3100 (vw), 3075 (vw), 3045 (vw), 3010 (w), 2720 (w), 1600 (s), 1571 (m), 1565 (w), 1550 (s), 1410 (m), 1315 (m), 1294 (s), 1278 (w), 1230 (m), 1215 (vs), 1195 (vw), 1155 (w), 1111 (vs), 1065 (s), 1020 (m), 990 (vw), 976 (s), 965 (vw), 916 (vs), 902 (vs), 825 (w), 800 (w), 760 (vs), 740 (vs), 708 (vs), 670 (m), 660 (m), 632 (m), 628 (w), 620 (vw), 579 (vw), 472 (s), 388 (s), 309 (vs).

Yb(C_5Me_5)$_2$(phthalazine) (3). A solution of phthalazine (0.17 g, 1.3 mmol) in 40 mL of diethyl ether was added to a solution of Yb(C_5Me_5)$_2$(OEt_2) (0.67 g, 1.3 mmol) in 20 mL of diethyl ether with rapid stirring. The deep red solution was stirred for 30 min and filtered, and the filtrate was concentrated to ca. 20 mL. Cooling at −10 °C produced fine red needles of **3**. Yield: 0.62 g (84%). Mp: >330 °C. Anal. Calcd for $C_{28}H_{36}N_2Yb$: C, 58.6; H, 6.33; N, 4.88. Found: C, 58.8; H, 6.41; N, 4.90. IR (cm^{-1}): 2720 (vw), 1590 (w), 1550 (w), 1360 (w), 1328 (m), 1300 (w), 1280 (m), 1211 (w), 1170 (w), 1123 (w), 1070 (vw), 1020 (w), 970 (w), 891 (s), 718 (vs), 680 (vw), 535 (vw), 470 (vw), 385 (w), 351 (w), 311 (vs).

Yb(C_5Me_5)$_2$(quinoxaline) (4). A solution of sublimed quinoxaline (0.10 g, 0.77 mmol) in 20 mL of diethyl ether was added to a solution of Yb(C_5Me_5)$_2$(OEt_2) (0.79 g, 1.5 mmol) in 30 mL of diethyl ether with rapid stirring. Immediate precipitation of a sparkling brown microcrystalline solid occurred. The precipitate was washed twice with pentane and dried under reduced pressure. Yield: 0.35 g (80%). Mp: >330 °C. Anal. Calcd for $C_{28}H_{36}N_2Yb$: C, 58.6; H, 6.33; N, 4.88. Found: C, 58.7; H, 6.57; N, 4.59. IR (cm^{-1}): 2720 (w), 1587 (w), 1531 (w), 1493 (vw), 1438 (vw), 1422 (vw), 1367 (vw), 1350 (vw), 1322 (m), 1272 (w), 1210 (m), 1148 (s), 1126 (s), 1076 (vw), 1060 (vw), 1021 (m), 961 (vs), 936 (w), 819 (vw), 779 (m), 771 (w), 744 (m), 722 (vw), 612 (vw), 598 (w), 542 (w), 411 (m), 375 (br m), 327 (w), 294 (br s).

Yb(C_5Me_5)$_2$(1,5-naphthyridine) (5). A solution of 1,5-naphthyridine (0.07 g, 0.6 mmol) in 10 mL of diethyl ether was added to a stirred solution of Yb(C_5Me_5)$_2$(OEt_2) (0.61 g, 1.2 mmol) in 40 mL of diethyl ether. A brown precipitate appeared immediately, but the solution was stirred for a further 2 h. The solid was collected by filtration, washed twice with hexane, and dried under reduced pressure. The resulting free-flowing powder was insoluble in toluene and diethyl ether and afforded glassy solids containing solvent from THF. Yield: 0.31 g (92%). Mp: >330 °C. Anal. Calcd for $C_{28}H_{36}N_2$Yb: C, 58.6; H, 6.33; N, 4.88. Found: C, 59.5; H, 6.43; N, 4.34. IR (cm^{-1}): 2720 (w), 1619 (s), 1569 (s), 1554 (s), 1489 (m), 1426 (m), 1349 (m), 1304 (vs), 1256 (m), 1224 (w), 1206 (m), 1156 (w), 1129 (m), 1100 (vw), 1081 (s), 1019 (m), 966 (m), 945 (w), 906 (vw), 859 (vw), 835 (vw), 817 (w), 796 (s), 776 (s), 758 (m), 743 (s), 704 (vw), 665 (vw), 651 (m), 631 (m), 600 (w), 565 (w), 492 (vw), 430 (w), 380 (br m), 303 (br vs), 250 (vw).

Yb(C_5Me_5)$_2$(1,8-naphthyridine) (6). A solution of 1,8-naphthyridine (0.12 g, 0.93 mmol) in 20 mL of toluene was added to a stirred solution of Yb(C_5Me_5)$_2$(OEt_2) (0.48 g, 0.93 mmol) in 30 mL of toluene with rapid stirring. The deep red solution was stirred for 2 h and filtered, and the filtrate was concentrated to 35 mL and cooled at −10 °C for several days. Fine red needles were isolated from the mother liquor by filtration, but these rapidly collapsed to a rust-colored powder on exposure to vacuum. Yield: 0.33 g (62%). Mp: 220 °C dec. Anal. Calcd for $C_{28}H_{36}N_2Yb$: C, 58.6; H, 6.33; N, 4.88. Found: C, 58.5; H, 6.48; N, 4.87. IR (cm^{-1}): 3062 (vw), 3030 (vw), 2720 (w), 1610 (vs), 1582 (vs), 1549 (m), 1520 (m), 1420 (vs), 1388 (m), 1350 (w), 1338 (s), 1300 (s), 1265 (m), 1253 (m), 1238 (m), 1210 (m), 1195 (w), 1179 (m), 1120 (m), 1100 (vs), 1050 (w), 1020 (w), 962 (w), 942 (w), 931 (s), 920 (w), 830 (w), 800 (w), 759 (vs), 722 (vs), 618 (w), 595 (w), 550 (m), 530 (vw), 520 (w), 498 (vw), 421 (m), 390 (m), 310 (s), 250 (s).

Yb(C_5Me_5)$_2$(4,4′-bipyridine) (7). A solution of Yb(C_5Me_5)$_2$(OEt_2) (0.45 g, 0.87 mmol) in 50 mL of diethyl ether was added to a solution of 4,4′-bipyridine (0.07 g, 0.4 mmol) in 10 mL of diethyl ether with rapid stirring. Immediate precipitation of a purple solid occurred. After it was stirred for 1 h, the suspension was allowed to settle and the supernatant was filtered off and discarded. The precipitate was washed twice with hexane and dried under reduced pressure to afford **7** as a purple pyrophoric powder. The powder was insoluble in toluene, hexane, diethyl ether, and THF. Carrying out the above reaction in toluene produces a stiff purple gel that collapses to **7** under vacuum. Yield: 0.25 g (93%). Mp: >330 °C. Anal. Calcd for $C_{30}H_{38}N_2Yb$: C, 60.1; H, 6.39; N, 4.67. Found: C, 58.0; H, 6.36; N, 5.22. IR (cm^{-1}): 3180 (vw), 3070 (vw), 2725 (w), 2550 (vw), 1720 (w), 1595 (vs), 1550 (s), 1495 (s), 1340 (m), 1279 (w), 1260 (m), 1215 (m), 1195 (s), 1160 (w), 1090 (m), 1035 (w), 1015 (s), 960 (vs), 795 (s), 770 (m), 750 (w), 718 (m), 695 (vw), 680 (vw), 650 (br w), 611 (vs), 590 (w), 570 (vw), 370 (br s), 290 (vs).

[Yb(C_5Me_5)$_2$]$_2$(2,2′-bipyrimidine) (8). A solution of Yb(C_5Me_5)$_2$(OEt_2) (1.2 g, 2.2 mmol) in 60 mL of toluene was added to a solution of 2,2′-bipyrimidine (0.18 g, 1.1 mmol) in 50 mL of toluene with rapid stirring. The reaction mixture immediately turned dark red-brown. After the mixture was stirred for 12 h, a red-brown crystalline precipitate had separated from the reaction mixture. The solution was filtered, and the filtrate was concentrated to ca. 50 mL. Cooling at −10 °C afforded black-brown needles that were collected and dried under reduced pressure. The mother liquors were concentrated to ca. 20 mL and cooled to −10 °C, producing a second crop of crystals. Yield: 1.1 g (90%). Mp: 305−308 °C. Anal. Calcd for $C_{55}H_{73}N_4Yb_2$: C, 58.1; H, 6.48; N, 4.93. Found: C, 58.0; H, 6.81; N, 5.01%. MS (CI): *m*/*z* 1044 [M]$^+$, 910 [M − C_5Me_5]$^+$, 775 [M − 2C_5Me_5]$^+$, 641 [M − 3C_5Me_5]$^+$, 507 [M − 4C_5Me_5]$^+$, 467 [Yb(C_5Me_5)(bpm)]$^+$, 443 [Yb(C_5Me_5)$_2$]$^+$. IR (cm^{-1}): 2725 (w), 2670 (w), 2480 (w), 1735 (w), 1672 (w), 1635 (w), 1605 (sh m), 1589 (vs), 1555 (w), 1365 (vs), 1270 (vs), 1160 (w), 1091 (s), 1040 (vs), 946 (m), 725 (m), 693 (m), 675 (s), 618 (s), 587 (w), 460 (w), 385 (m), 303 (s), 242 (w).

[Yb(C_5Me_5)$_2$]$_2$(phenazine) (9). A solution of phenazine (0.07 g, 0.4 mmol) in 20 mL of diethyl ether was added to a solution of Yb(C_5Me_5)$_2$(OEt_2) (0.42 g, 0.81 mmol) in 20 mL of diethyl ether. The deep red solution was stirred for 15 min and then cooled at −10 °C overnight. Fine red crystals of **9** were isolated by filtration. Yield: 0.38 g (87%). Mp: > 330 °C. Anal. Calcd for $C_{52}H_{68}N_2Yb$: C, 58.5; H, 6.42; N, 2.62. Found: C, 58.2; H, 6.51; N, 2.62. IR (cm^{-1}): 3056 (vw), 2727 (w), 2620 (vw), 1860 (vw), 1596 (s), 1555 (w), 1330 (vs), 1306 (w), 1282 (vs), 1233 (w), 1213 (s), 1164 (vw), 1128 (m), 1052

(vw), 1023 (w), 896 (vs), 800 (vw), 749 (vw), 720 (vs), 685 (vw), 591 (w), 385 (br m), 354 (w), 315 (br vs), 280 (vw).

Yb(C_5Me_5)$_2$(azobenzene) (10). A solution of azobenzene (0.40 g, 2.2 mmol) in 20 mL of pentane was added to a suspension of Yb(C_5Me_5)$_2$(OEt_2) (1.15 g, 2.22 mmol) in 60 mL of pentane with stirring. The deep blue-green solution was stirred for 1 h, the solution was filtered, and the filtrate was concentrated to 10 mL. Cooling at −20 °C for several days afforded dark blue-green crystals by filtration. Further cooling of the filtrate at −78 °C afforded a second crop of crystals. Yield: 0.65 g (47%). Mp: 164−167 °C. Anal. Calcd for $C_{32}H_{40}N_2Yb$: C, 61.4; H, 6.44; N, 4.47. Found: C, 61.6; H, 6.48; N, 4.53%. MS (CI): *m*/*z* 626 [M]$^+$, 491 [M − C_5Me_5]$^+$, 444 [Yb(C_5Me_5)$_2$]$^+$, 183 [PhNNPh]$^+$, 135 [C_5Me_5]$^+$. IR (cm^{-1}): 3080 (w), 3050 (w), 2730 (w), 1905 (vw), 1855 (vw), 1835 (vw), 1765 (vw), 1580 (s), 1560 (m), 1341 (m), 1324 (vw), 1300 (w), 1282 (vw), 1227 (m), 1161 (w), 1151 (w), 1091 (s), 1075 (m), 1018 (s), 986 (m), 975 (w), 884 (w), 879 (m), 819 (w), 783 (s), 750 (vs), 711 (s), 680 (vs), 571 (m), 525 (m), 516 (w), 489 (w), 380 (s), 314 (vs).

[Yb(C_5Me_5)$_2$]$_2$(azobenzene) (11). A solution of azobenzene (0.20 g, 1.2 mmol) in 30 mL of pentane was added to a suspension of Yb(C_5Me_5)$_2$(OEt_2) (1.2 g, 2.3 mmol) in 50 mL of pentane with stirring. The initially blue-green solution slowly changed color to deep purple over the course of 1 h. The purple-black solution was stirred for 4 h and filtered, and the filtrate was concentrated to 10 mL. Cooling at −78 °C produced small dark purple prisms. Yield: 0.25 g (20%). Mp: 195−197 °C. Anal. Calcd for $C_{52}H_{70}N_2Yb_2$: C, 58.4; H, 6.60; N, 2.62. Found: C, 57.9; H, 6.64; N, 2.55. IR (cm^{-1}): 2725 (w), 1582 (s), 1530 (m), 1330 (m), 1296 (m), 1272 (w), 1176 (br m), 1096 (w), 1020 (s), 969 (m), 948 (vw), 929 (vw), 850 (w), 820 (w), 797 (w), 750 (w), 730 (vs), 708 (w), 620 (m), 590 (vw), 580 (m), 531 (w), 511 (vw), 500 (w), 423 (w), 380 (br m), 299 (br s), 275 (w).

[Yb(C_5Me_5)$_2$]$_2$(2,2′-azopyridine) (12). A solution of 2,2′-azopyridine (0.18 g, 0.98 mmol) in 20 mL of toluene was added to a solution of Yb(C_5Me_5)$_2$(OEt_2) (1.03 g, 1.99 mmol) in 40 mL of toluene with stirring. The red-brown solution was stirred for 1 h and filtered by cannula and the filtrate concentrated to 40 mL. Cooling at −10 °C overnight afforded **12** as large dark brown crystals. Yield: 0.80 g (75%). Mp: >330 °C. Anal. Calcd for $C_{50}H_{68}N_4Yb_2$: C, 56.1; H, 6.40; N, 5.23. Found: C, 56.5; H, 6.47; N, 5.19. MS (EI): *m*/*z* 1072 [M]$^+$, 937 [M − C_5Me_5]$^+$, 802 [M − 2 C_5Me_5]$^+$, 666 [M − 3 C_5Me_5]$^+$, 531 [M − 4 C_5Me_5]$^+$, 358 [Yb(2,2′-azopyridine)]$^+$. IR (cm^{-1}): 2722 (w), 1601 (vs), 1558 (w), 1523 (m), 1479 (vs), 1465 (vs), 1296 (m), 1275 (w), 1210 (w), 1156 (m), 1097 (w), 1063 (vw), 1022 (m), 988 (vs), 838 (vw), 800 (w), 774 (w), 751 (s), 723 (m), 648 (w), 623 (w), 584 (w), 556 (w), 519 (w), 413 (w), 378 (br m), 350 (w), 301 (br vs).

[Yb(C_5Me_5)$_2$]$_2$(2,3-bis(2′-pyridino)quinoxaline) (13). A solution of Yb(C_5Me_5)$_2$(OEt_2) (0.67 g, 1.3 mmol) in 250 mL of pentane was added to a Schlenk flask containing 2,3-bis(2′-pyridino)quinoxaline (0.18 g, 0.63 mmol) with rapid stirring. The green-black mixture was stirred for 1 h, after which time no solids remained. Filtration and concentration of the filtrate to 50 mL followed by cooling at −10 °C for several days produced shiny black needles of **13**. Yield: 0.41 g (61%). Mp: >330 °C. Anal. Calcd for $C_{58}H_{72}N_4Yb_2$: C, 59.5; H, 6.20; N, 4.78. Found: C, 55.8; H, 6.20; N, 4.31. IR (cm^{-1}): 3050 (w), 2715 (w), 1718 (w), 1585 (m), 1560 (m), 1533 (m), 1420 (w), 1333 (m), 1310 (m), 1272 (m), 1251 (m), 1240 (w), 1210 (w), 1191 (m), 1162 (w), 1155 (w), 1140 (s), 1096 (s), 1072 (w), 1046 (w), 1020 (w), 1008 (w), 970 (vs), 852 (m), 798 (br s), 775 (w), 768 (s), 732 (s), 712 (s), 702 (s), 639 (w), 610 (w), 550 (vs), 472 (br m), 430 (m), 355 (w), 305 (vs).

Magnetic Susceptibility Measurements. Magnetic susceptibility measurements were made using an S.H.E. Model 905 superconducting magnetometer (SQUID). Sample containers made from tightly fitting Kel-F halves were used for air-sensitive samples; no significant decomposition was noted during the course of measurement (typically ca. 24 h). In a standard experiment, 50−75 mg of the compound to be studied was finely ground and weighed into a Kel-F container in an argon-filled drybox. The halves of the container were sealed with the aid of a thin film of silicone grease. After removal from the drybox, the container was wired together with nylon monofilament thread and suspended in the sample chamber by a cotton thread. The sample chamber was then alternately evacuated to 30 μm of mercury pressure and refilled with high-purity helium three times. Samples were measured automatically at two fields (5 and 40 kG) at temperatures from 5 to 300 K using the following temperature steps: 3 K from 5 to 21 K; 5 K from 25 to 50 K; 10 K from 50 to 100 K; 20 K from 100 to 300 K. Sample data were corrected for container (including grease) and sample diamagnetism. Samples exhibiting Curie−Weiss behavior were fit to the Curie−Weiss law using a linear least-squares program. Effective magnetic moments were then calculated from the slope of the linear regions using $\mu = 2.828C^{1/2}$.

X-ray Crystallographic Studies. Crystals of 2,2′-bipyrimidine were grown by sublimation at 90 °C and 10^{-2} Torr. Large crystals of **8** were grown from toluene solution and cut under an argon atmosphere. In both cases, the crystals were lodged in a quartz capillary and flame-sealed prior to analysis. Preliminary precession photographs indicated triclinic Laue symmetry for **8**, while the space group for 2,2′-bipyrimidine was uniquely determined to be $P2_1/n$ (monoclinic). The crystals were mounted and centered on a CAD4 diffractometer, and the cell dimensions were established by a least-squares fit of 24 independent high-angle reflections (2,2′-bipyrimidine, 2θ = 22−32°; **8**, 2θ = 27−31°). Data collection was performed at room temperature for **8** and at −110 °C for 2,2′-bipyrimidine. Raw data were corrected for scan speed, background, and Lorentz−polarization effects.[37,38] An analytical absorption correction was also applied to **8** (maximum/minimum transmission factors 0.522, 0.445). An azimuthal scan showed no variation in intensity for 2,2′-bipyrimidine; thus, no absorption correction was applied.[39] Initial structure solutions were obtained using MULTAN (2,2′-bipyrimidine) or Patterson methods (**8**).

Full-matrix least-squares refinement proceeded normally for 2,2′-bipyrimidine. The least-squares procedure minimized $\sum w(|F_o| - |F_c|)^2$, where w is the weight of a given reflection. The analytical forms of the scattering factors for the neutral atoms[40] were used, and all non-hydrogen scattering factors were corrected for anomalous dispersion.[41] Low-angle, high-intensity reflections showed signs of secondary extinction and were therefore corrected for this effect.[42] All hydrogen atoms were located in the difference map and were refined isotropically; non-hydrogen atoms were refined anisotropically. The largest peak in the final difference Fourier map had an electron density of 0.36 e Å^{-3}.

(37) *Structure Determination Package User's Guide*; B. A. Frenz and Associates: College Station, TX 77840, 1982.

(38) The data reduction formulas are $F_o^2 = \omega(C - 2B)$/Lp, $F_o = (F_o^2)^{1/2}$, $\sigma_o(F_o^2) = \omega(C + 4B)^{1/2}$/Lp, and $\sigma_o(F) = \sigma_o(F_o^2)/(2F_o)$ where C is the total count in the scan, B is the sum of two background counts, ω is the scan speed in deg/min, and $Lp^{-1} = \{\sin 2\theta(1 + \cos^2 2\theta_m)\}/\{1 + \cos^2 2\theta - \sin^2 2\theta\}$ is the correction for Lorentz and polarization effects for a reflection with scattering angle $2r$ and radiation monochromatized with a 50% perfect single-crystal monochromator with scattering angle $2r_m$.

(39) Reflections used for azimuthal scans were located near $\chi = 90°$, and the intensities were measured at 10° increments of rotation of the crystal about the diffractometer vector.

(40) Cromer, D. T.; Waber, J. T. *International Tables for X-ray Crystallography*; Kynoch Press: Birmingham, U.K., 1974; Vol. IV, Table 2.2B.

(41) Cromer, D. T.; Waber, J. T. *International Tables for X-ray Crystallography*; Kynoch Press: Birmingham, U.K., 1974; Vol. IV, Table 2.3.1.

(42) Zachariesen, W. H. *Acta Crystallogr.* **1963**, *16*, 1139.

The refinement of **8** did not proceed smoothly, due to two different types of disorder. The first type of disorder involved the toluene of solvation present in the lattice. The disorder of the toluene molecules was modeled using two half-occupancy molecules that were refined as constrained isotropic bodies. The C−C−C angles were constrained to 120°, while the C_{ring}−C_{ring} and C−Me bond lengths were fixed at 1.40 and 1.50 Å, respectively. Attempts to refine this model still resulted in very poor thermal parameters for the methyl group on one of the rigid units; therefore, this group was ultimately removed in the final structure refinement.

The second type of disorder involved rotational disorder for three of the four C_5Me_5 rings. The methyl carbons of each disordered ring resolved into 10 half-occupancy groups, while the ring carbons themselves could not be resolved. Each disordered ring was modeled using two half-occupancy C_5Me_5 rings that were refined as rigid isotropic bodies. The C_{ring}−C_{ring} and C−Me distances were constrained to 1.42 and 1.50 Å, respectively. The ring C−C−C and C−C−Me angles were constrained to 108 and 126°, respectively. The initial position of the ring carbons was calculated from the position of its attached methyl group. Each C_5Me_5 ring was refined independently, and this resulted in the observed variation in the Yb−C_{ring} bond lengths (see the Supporting Information).

Full matrix least-squares refinement proceeded satisfactorily for **8** when the constraints described above were implemented. The least-squares procedure minimized $\sum w(|F_o| - |F_c|)^2$, where w is the weight of a given reflection. The analytical forms of the scattering factors for the neutral atoms[40] were used, and all non-hydrogen scattering factors were corrected for anomalous dispersion.[41] Low-angle, high-intensity reflections showed signs of secondary extinction, and given the large extinction coefficient calculated (2.57×10^{-7}), it was included even though the H atoms were not included in the structure factor calculations.[42] The largest peak in the final difference Fourier map had an electron density of 0.73 e Å^{-3}.

Acknowledgment. This work was partially supported by the Director, Office of Basic Energy Research, Office of Basic Energy Sciences, Chemical Sciences Division, of the U.S Department of Energy under Contract No. DE-AC03-76SF00098. We thank Dr. Fred Hollander for his help with the crystallography, the NSERC of Canada for a fellowship to D.J.B., and Evan Werkema for his help with the figures.

Supporting Information Available: Tables of atomic coordinates, all bond distances and angles, and anisotropic thermal parameters for both structures. This material is available free of charge via the Internet at http://pubs.acs.org. Structure factor tables are available from the authors.

OM020477E